Cell Reports
Report

Cryoelectron Microscopic Structures of Eukaryotic Translation Termination Complexes Containing eRF1-eRF3 or eRF1-ABCE1

Anne Preis,[1,2] Andre Heuer,[1,2] Clara Barrio-Garcia,[1,2] Andreas Hauser,[1,2] Daniel E. Eyler,[3,4] Otto Berninghausen,[1,2] Rachel Green,[3,4] Thomas Becker,[1,2,*] and Roland Beckmann[1,2,*]
[1]Gene Center Munich, Department of Biochemistry, Feodor-Lynen-Strasse 25, University of Munich, 81377 Munich, Germany
[2]Center for Integrated Protein Science Munich, Department of Biochemistry, Feodor-Lynen-Strasse 25, University of Munich, 81377 Munich, Germany
[3]Howard Hughes Medical Institute, Chevy Chase, MD 20815-6789, USA
[4]Department of Molecular Biology and Genetics, Johns Hopkins University School of Medicine, Baltimore, MD 21205, USA
*Correspondence: becker@lmb.uni-muenchen.de (T.B.), beckmann@lmb.uni-muenchen.de (R.B.)
http://dx.doi.org/10.1016/j.celrep.2014.04.058

SUMMARY

Termination and ribosome recycling are essential processes in translation. In eukaryotes, a stop codon in the ribosomal A site is decoded by a ternary complex consisting of release factors eRF1 and guanosine triphosphate (GTP)-bound eRF3. After GTP hydrolysis, eRF3 dissociates, and ABCE1 can bind to eRF1-loaded ribosomes to stimulate peptide release and ribosomal subunit dissociation. Here, we present cryoelectron microscopic (cryo-EM) structures of a pretermination complex containing eRF1-eRF3 and a termination/prerecycling complex containing eRF1-ABCE1. eRF1 undergoes drastic conformational changes: its central domain harboring the catalytically important GGQ loop is either packed against eRF3 or swung toward the peptidyl transferase center when bound to ABCE1. Additionally, in complex with eRF3, the N-terminal domain of eRF1 positions the conserved NIKS motif proximal to the stop codon, supporting its suggested role in decoding, yet it appears to be delocalized in the presence of ABCE1. These results suggest that stop codon decoding and peptide release can be uncoupled during termination.

INTRODUCTION

Translation termination and ribosome recycling are essential processes in ribosome-driven protein synthesis triggered by the appearance of a stop codon in the A site of the ribosome during elongation. In the first stage of this cycle, the release factor (RF) eRF1 is delivered to the ribosome by the guanosine triphosphatase (GTPase) eRF3, which departs following guanosine triphosphate (GTP) hydrolysis. Next, ABCE1 binds to the factor-binding site of ribosomes loaded with eRF1 and facilitates peptide release and then subunit dissociation. These events are tightly coordinated through their common utilization of eRF1 (Pisarev et al., 2010; Shoemaker et al., 2010; Shoemaker and Green, 2011).

To date, several X-ray and cryoelectron microscopic (cryo-EM) structures exist for individual eRFs as well as unbound and ribosome-bound eRF1-eRF3 complexes (Cheng et al., 2009; des Georges et al., 2014; Kong et al., 2004; Song et al., 2000; Taylor et al., 2012). Recent cryo-EM structures of a rabbit pretermination complex show eRF1 trapped in the process of delivery to the ribosome by eRF3 bound to the nonhydrolyzable GTP analog guanylyl imidodiphosphate (GDPNP). As a result, the catalytically essential GGQ motif of eRF1 is positioned approximately 90 Å apart from the peptidyl transferase center (PTC) where peptide release is ultimately catalyzed. Therefore, it remains an open question what the active conformation of eRF1 on the terminating ribosome might be. Moreover, whereas it has previously been shown that ABCE1 can stimulate eRF1-dependent peptide release before dissociating ribosomes into subunits, thereby coupling translation termination with ribosome recycling (Shoemaker and Green, 2011), we have little structural understanding of these processes.

Important clues regarding the possible behavior of eRF1 and eRF3 come from the closely related mRNA surveillance (or ribosome rescue) factors Pelota (Dom34p in yeast) and Hbs1. These factors are paralogs of eRF1 and eRF3, recognize stalled ribosomes, and initiate subsequent ribosome rescue/recycling together with ABCE1 that ends in degradation of aberrant mRNA and proteins (Barthelme et al., 2011; Doma and Parker, 2006; Pisareva et al., 2011; Shoemaker and Green, 2011). Cryo-EM structures of stalled ribosomes in complex with Pelota and either Hbs1 or ABCE1 showed that the central domain of Pelota undergoes a dramatic conformational change in these different complexes. In the prerescue state (in the presence of Hbs1:GDPNP), Pelota is packed against Hbs1 and not fully engaged in the A site, whereas in the recycling complex bound to ABCE1:adenylyl imidodiphosphate (ADPNP), Pelota stretches out within the A site reaching toward the P site-tRNA (Becker et al., 2011, 2012; Franckenberg et al., 2012). Based on the

homology between these rescue factors and eukaryotic-RFs, similar behavior of eRF1 may explain how ABCE1 exerts its influence on peptide release. However, direct structural evidence for this model is not available so far.

RESULTS AND DISCUSSION

Generation and Cryo-EM of Pretermination and Termination/Prerecycling Complexes

Stable ribosomal complexes bound to eRF1 and eRF3 or ABCE1 were generated by employing a stalling polypeptide sequence from the human cytomegalovirus (CMV) *gp48* uORF. This peptide sequence stalls translation by inhibiting eRF1-mediated peptide release with a UAA stop codon-programmed ribosomal A site (Bhushan et al., 2010; Janzen et al., 2002). The detailed molecular changes responsible for prohibiting peptide release by eRF1 and also puromycin activity in this seemingly normal ribosomal termination complex are not known (Figure S1A).

We used a wheat germ in vitro translation system to generate CMV-stalled ribosome-nascent chain complexes (RNCs) (Bhushan et al., 2010) and then added either purified recombinant *Saccharomyces cerevisiae* eRF1-eRF3:GDPNP (Sup45p-Sup35p) ternary complex or eRF1 and ABCE1:ADPNP. eRF3 lacks the prion-forming domain (N-terminal 97 amino acids) that has been shown to be nonessential for termination activity in yeast (Alkalaeva et al., 2006; Frolova et al., 1996). To test the functional activity of these heterologous complexes, we performed release assays where we followed peptide release by immunodetection of the HA-tagged peptidyl tRNA and free peptide. In this case, the CMV-stalled RNCs were directly compared with RNCs prepared on a truncated mRNA. Although peptide was quantitatively released from the peptidyl tRNA by puromycin on the truncated mRNA RNCs, the CMV-stalled RNC peptides were substantially less reactive with puromycin (Figure S1A). These data confirmed the known downregulation of the PTC by the CMV-stalling peptide. Similarly, as expected, neither eRF1 alone nor in conjunction with eRF3 displayed detectable release activity with the CMV RNCs. Interestingly, eRF1 and ABCE1 together resulted in a detectable increase in the relative amounts of free peptide, consistent with earlier studies showing a stimulation of peptide release by ABCE1 (Shoemaker and Green, 2011). This limited peptide-release activity provides support for the functional relevance of the heterologous ribosome complexes analyzed in this manuscript.

We performed cryo-EM and single-particle analysis including in silico sorting procedures to obtain structures of CMV RNC-eRF1-eRF3:GDPNP and CMV RNC-eRF1-ABCE1:ADPNP at a resolution of 9.15 and 8.75 Å at a Fourier shell correlation (FSC) cutoff of 0.5, respectively (8.9 and 8.6 Å at a FSC cutoff at 0.143 after processing according to the so-called gold standard approach) (Figures 1A, S1B, and S1C). For molecular interpretation, we used an updated model of the *Triticum aestivum* ribosome (Gogala et al., 2014) and placed homology models of eRF1, eRF3, and ABCE1 in the assigned densities, where most secondary structure was resolved. This was validated by calculating the cross-resolution between the models and the maps (Figures 1B and S2).

The pretermination complex showed extra densities for eRF1-eRF3 and P site-tRNA in positions consistent with previous observations in the rabbit eRF1:eRF3 pretermination complex (des Georges et al., 2014; Taylor et al., 2012) and in the yeast RNC-Pelota-Hbs1-complex (Becker et al., 2011). eRF1 is located in the A site, and its N-terminal domain (NTD) reaches into the decoding center of the small ribosomal subunit (SSU). The C-terminal domain (CTD) and central domain of eRF1 are packed against eRF3, which binds the ribosome like a classical EF-Tu-like translational GTPase. No density could be identified for the NTD of eRF3 (residues 97–255), suggesting a relatively flexible nature for this domain in our complex.

The termination/prerecycling complex showed dramatic conformational changes wherein eRF1 stretches between the P site-tRNA and ABCE1 that is located in the same position as seen previously in the Pelota ribosome complex (Becker et al., 2012). The CTD of eRF1 contacts the iron-sulfur (FeS) domain of ABCE1, whereas the central domain bearing the GGQ motif is stretched out toward the PTC of the large ribosomal subunit (LSU) where it contacts the P site-tRNA at the CCA end. Surprisingly, density for the NTD of eRF1 appeared to be fragmented and can only be visualized when the map is low-pass filtered at around 20 Å. This behavior is indicative of increased flexibility or disorder in this region that we confirmed in analysis of difference maps (Figure S3).

The Pretermination Complex

As mentioned briefly above, in the CMV RNC-eRF1-eRF3 pretermination complex, the ribosome adopts a similar overall conformation as observed for a stalled ribosome with Pelota-Hbs1 harboring a P site-tRNA (Becker et al., 2011) and the mammalian pretermination complex containing eRF1 and eRF3 (des Georges et al., 2014).

Consistent with the rabbit pretermination complex, the main contacts between eRF1 and the ribosome are found between the SSU and the NTD of eRF1 (Figure 2; Table S1). The conserved (TAS)NIKS loop is proximal to the stop codon poised in the A site, consistent with its critical role in stop codon recognition (Figure 2C). The NIKS loop is located in a similar position relative to the stop codon as for the equivalent loop (PVT/SPF) in bacterial RF1/RF2 that is involved in decoding (Korostelev et al., 2008; Laurberg et al., 2008; Weixlbaumer et al., 2008).

Density for the NTD of eRF1 was not defined clearly enough as to allow for unambiguous positioning of the mRNA and individual residues of the (TAS)NIKS motif. Conformational changes of the NTD upon ribosome binding and during the event of decoding have indeed been postulated on the basis of toeprinting and chemical-crosslinking assays (Alkalaeva et al., 2006; Kryuchkova et al., 2013). In a previously proposed two-step model, recognition of the first two nucleotides in the codon is followed by a conformational change of the NTD of eRF1 that allows for decoding of the second and third nucleotides (Kryuchkova et al., 2013). The existence of distinct somewhat different conformations of eRF1 in this region might explain the limited resolution of the NTD during decoding in our structure.

The contacts between the CTD of eRF1 and domain III of eRF3 are formed by similar structural elements as previously reported in the crystal structure of human eRF1-eRF3 complex (Cheng

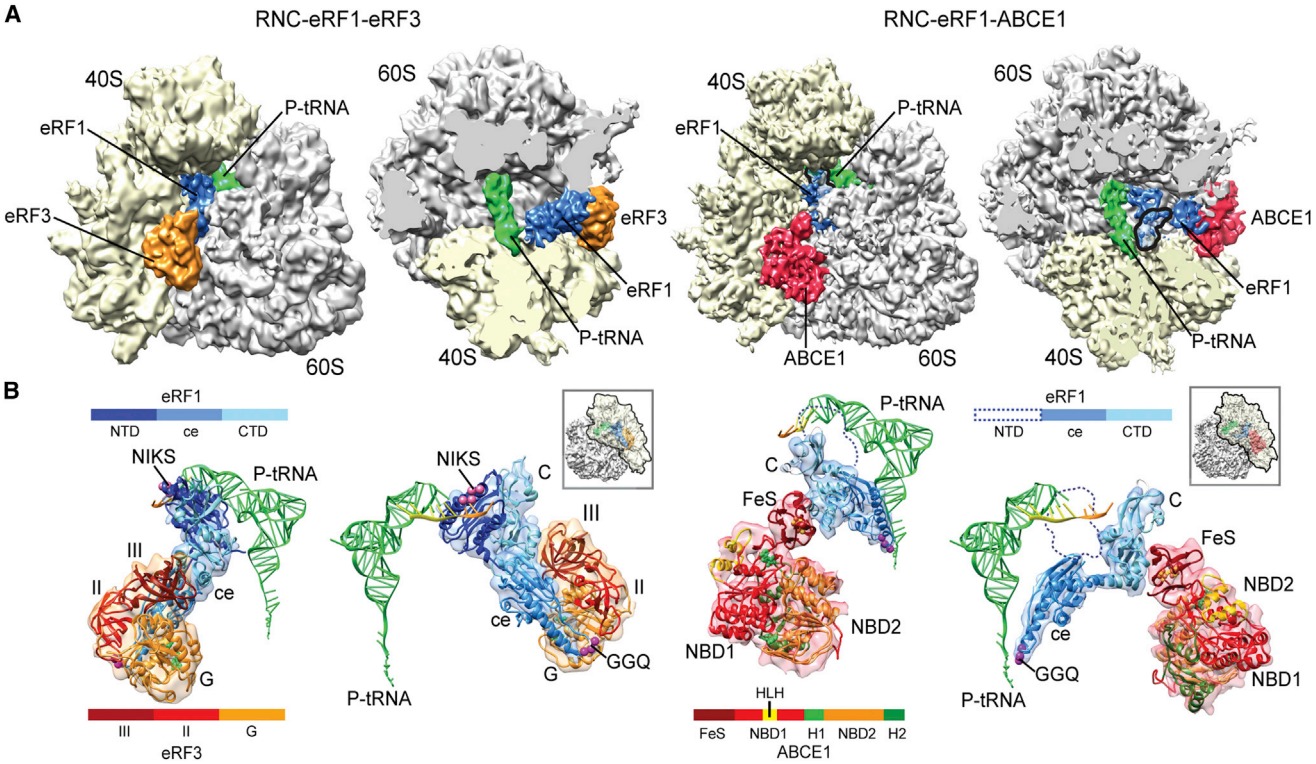

Figure 1. Cryo-EM Structures of Pretermination and Termination/Prerecycling Complexes

(A) Side and top views of the 80S ribosome pretermination complex with eRF1 and eRF3 (left) and termination/prerecycling complex with eRF1-ABCE1 (right). Density attributed to eRF1 occupies the A site. In the termination/prerecycling complex, the position of the flexible NTD of eRF1 is outlined with a black line.

(B) Molecular models for peptidyl tRNA, eRF1, eRF3, and ABCE1 on the ribosome. The NIKS motif (pink spheres) of eRF1 is positioned in close proximity to the stop codon (orange). The central domain of eRF1 containing the GGQ loop (magenta spheres) is packed against eRF3. In complex with ABCE1, the central domain of eRF1 is swung toward the PTC.

et al., 2009). Here, however, helices α8 and α11 even more closely contact domain III of eRF3 (Figure S4). The minidomain in the CTD of eRF1 (that is only present in the nuclear magnetic resonance structure in the CTD of eRF1; Mantsyzov et al., 2010) anchors eRF1 to the beak of the SSU via the rRNA expansion segment ES8 and ribosomal protein (r-protein) S31. The central domain of eRF1 is tightly packed against all three domains of eRF3 and forms a large interaction surface of 1,088 Å^2. As such, both the switch I and switch II regions of the G domain of eRF3 are in contact with eRF1 (Figure S4; Table S1).

Notably, we also observe a few differences when comparing our structure to the RNC-Pelota-Hbs1 structure or the rabbit pretermination complex. In our structure, the inward movement of the stalk base compared to the factor-free state (rRNA helices H43 and H44 and r-protein L11, according to the nomenclature introduced by Jenner et al., 2012) is less pronounced (Figure S4). Concomitantly, the central domain and the CTD (including the minidomain) of eRF1 as well as eRF3 are bound in a more outward position such that the central domain of eRF1 is positioned closer to the small subunit and even contacts rRNA helix h14 with helix α5 that directly connects to the GGQ loop (Figure 2A; Table S1). As a result, the functionally critical GGQ loop is sandwiched between the G domain of eRF3 and the SSU in a tightly locked conformation that is incompatible with peptide-release activity at this pretermination stage. In order to be active for release, a dramatic conformational change is needed to position the GGQ motif of the eRF1 central domain in the peptidyl-transferase center.

The Termination/Prerecycling Complex

The overall conformation of the ribosome in the CMV RNC-eRF1-ABCE1 complex is indeed similar to that observed in the RNC-Pelota-ABCE1 complex (Becker et al., 2012). In both cases, the stalk base is moved downward toward the sarcin-ricin loop (SRL; H95) (Figure S4B), and as in the pretermination complex, we observe P site-tRNA and a nascent peptide in the ribosomal exit tunnel, indicating that minimal if any peptide release has occurred in this particle population (Figure 3B).

The conformation of ABCE1 bound to the ribosome was also remarkably similar when compared to the Pelota-ABCE1-containing complex. ABCE1 binds in the translation factor-binding site and adopts an intermediate conformation of its nucleotide-binding domains (NBDs), somewhere between a fully open, ADP-bound structure, and the proposed closed ATP-bound form (Becker et al., 2012; Karcher et al., 2008). ABCE1 contacts the small subunit (h5-h15, h8-h14) mainly via its unique helix-loop-helix (HLH) and hinge motifs. Additional contacts are observed between NBD2 and L10.

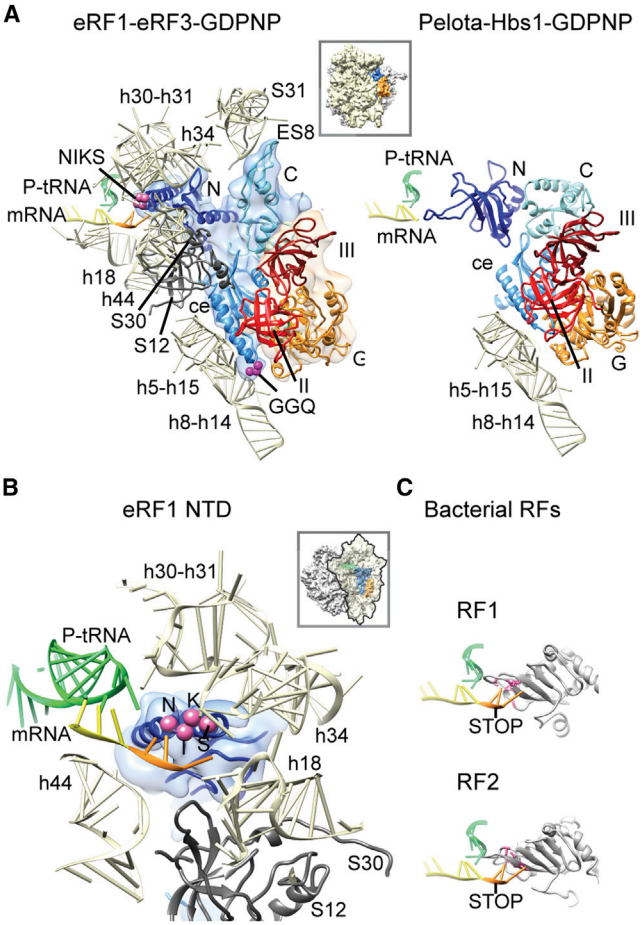

Figure 2. eRF1-Ribosome Interactions and Positioning of the NTD of eRF1 in the Pretermination Complex

(A) eRF1 forms multiple contacts with the ribosome (left) that are mostly identical to those of Pelota in complex with Hbs1 (right) (Becker et al., 2011), apart from a contact at h8-h14 of the 18S rRNA. The minidomain of the CTD of eRF1 contacts ES8 and S31 near the beak of the SSU.

(B) The NTD reaches deep into the decoding center and establishes multiple contacts with 18S rRNA and S12 (left). The NIKS motif is close to the stop codon in the A site (orange).

(C) For decoding of the stop codon, bacterial RF1 and RF2 (Korostelev et al., 2008; Laurberg et al., 2008) rely on domain II that is unrelated to eRF1 NTD. Interacting amino acids are marked in pink.

Notably, eRF1 adopts a dramatically changed elongated conformation similar to ribosome-bound Pelota in the presence of ABCE1 (Figure 3). This elongated conformation is broadly similar to that of bacterial ribosome-bound RFs (Korostelev et al., 2008; Laurberg et al., 2008; Weixlbaumer et al., 2008), though in contrast to the bacterial structures, the NTD (the codon-interaction domain) of eRF1 appears to be delocalized.

The CTD of eRF1 contacts the FeS domain of ABCE1, the stalk base (H43-H44 and L11), and the SRL (H95) in the LSU. The central domain of eRF1 undergoes the most drastic conformational rearrangements in this structure, establishing multiple contacts to the rRNA (H71, H89, H91, H92, and H93) and stretching out toward the P site-tRNA. The conserved loop containing the GGQ motif is now located at the PTC of the LSU in close proximity to the CCA end of the peptidyl tRNA (Table S2). Modeling the GGQ region on the basis of previous crystal structures of bacterial RF1 and RF2 bound to the ribosome allowed for easily fitting of the density without further adjustments (Figure 3B). Although eRF1 is otherwise unrelated in sequence and structure (the class 1 RFs evolved independently in these two lineages), this structural finding suggests that the strictly conserved GGQ motif functions in the same way in these two systems.

Finally, we see stabilization of eRF1 in this active conformation by ABCE1 through contacting the CTD of eRF1. These structural observations rationalize how this ATPase can stimulate eRF1-dependent peptide-release activity (Shoemaker and Green, 2011). In order to fully appreciate the contribution that ABCE1 makes to positioning of eRF1 for catalysis, however, it will be useful to determine the structure of a ribosome complex loaded with eRF1 alone.

Conclusions

Our cryo-EM structures show that eukaryotic termination and ribosome recycling by eRF1, eRF3, and ABCE1 follow the same order of events and conformational transitions as observed previously for stalled ribosome rescue by Pelota, Hbs1, and ABCE1. In both pathways, the A site factor, eRF1 for termination and Pelota for ribosome rescue, is delivered by the EF-Tu-like GTPase eRF3 or Hbs1, respectively, which then dissociates from the ribosome after GTP hydrolysis (Figure 4). In their pre-GTP hydrolysis state, eRF1-eRF3 and Pelota-Hbs1 adopt similar conformations on the ribosome, though in the pre-termination (eRF1) complex, an additional prominent contact between the central domain of eRF1 and the SSU is established; as a consequence, this domain is more tightly locked between the SSU and eRF3. Notably, the central domain of eRF1 contacts both the switch I and switch II regions of eRF3 that control its GTP hydrolysis. Higher-resolution structures will be required to decipher how decoding of the stop codon coordinates these events on a molecular level.

Next, we see that after eRF3 dissociation, eRF1 changes its conformation such that the central domain of eRF1 moves toward the PTC for catalysis of peptide release. The ribosome-eRF1 complex allows for binding of ABCE1 that appears to stabilize the fully extended active conformation of eRF1, thereby stimulating peptide release (Movie S1). Interestingly, the NTD of eRF1 appears to disengage the A site codon in this complex, indicating that codon engagement may not be required at this stage for peptide release. Yet, in contrast to the bacterial RFs that dissociate after termination (Freistroffer et al., 1997), eRF1 is still required for ABCE1-dependent ribosomal subunit splitting (Pisarev et al., 2010; Shoemaker and Green, 2011).

In a final stage, we know that ABCE1 functions in concert with bound eRF1 (on the posttermination complex) to promote subunit dissociation (Pisarev et al., 2010; Shoemaker and Green, 2011). Here, we see that ABCE1 adopts a remarkably similar conformation as observed in the prerecycling complex with Pelota (Becker et al., 2012). These data indicate that the mechanism of 80S splitting follows the same principle, independent of the nature of the ribosome to be recycled. Like Pelota in the context of ribosome rescue, eRF1 may act as a structural

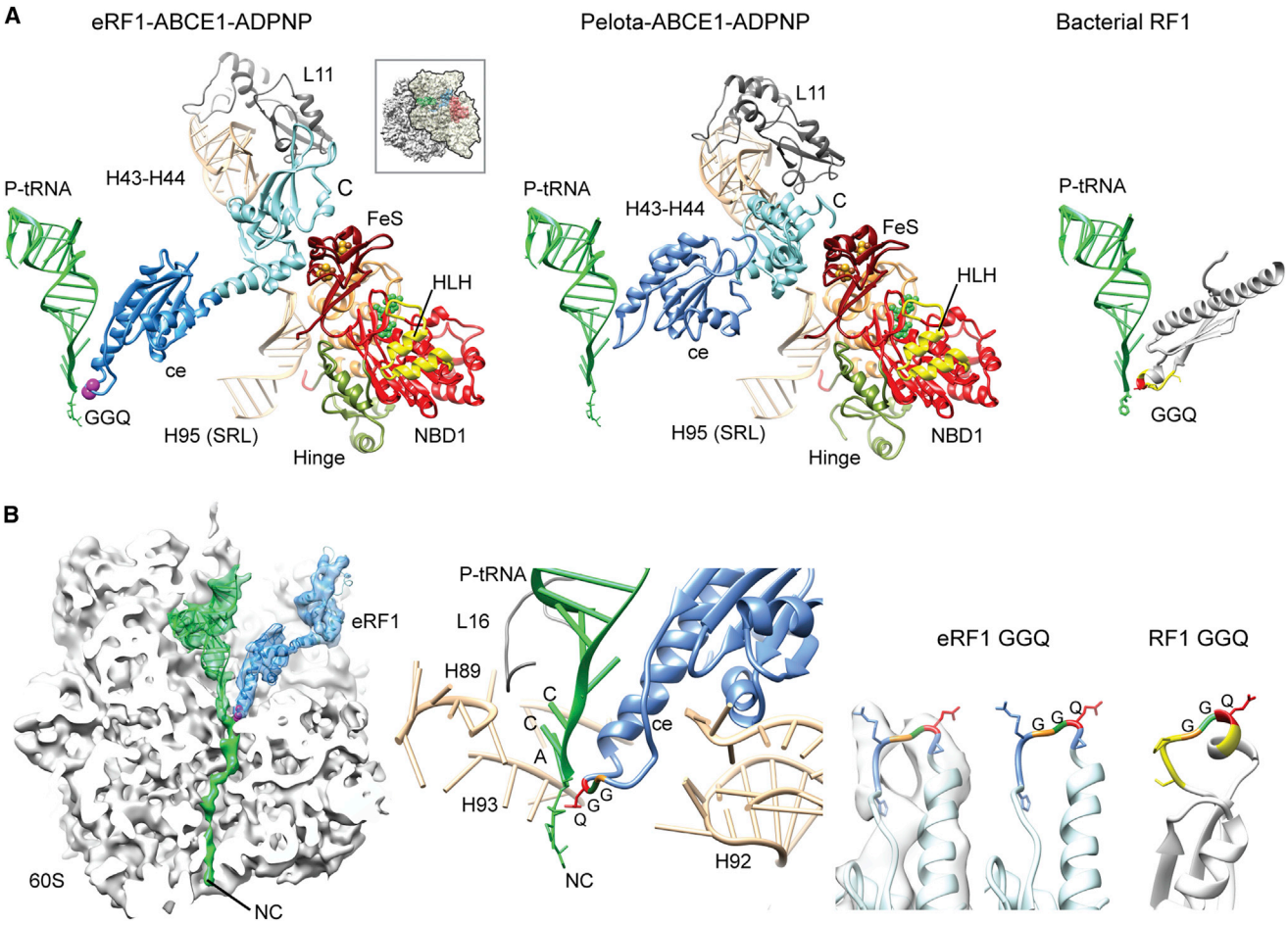

Figure 3. eRF1 Interactions and Positioning of Its Central Domain in the Termination/Prerecycling Complex

(A) The central domain of eRF1 undergoes a conformational change that positions the GGQ loop near the CCA end of the P site-tRNA (left). The CTD moves away from the SSU and forms contacts with the stalk base of the LSU and the SRL. These conformational changes are very similar to those of Pelota in complex with ABCE1 (middle). Unrelated domain III of bacterial RF1 possesses a different architecture but coordinates the highly conserved GGQ loop in an identical position (right).

(B) Cross-section and close-up view of the central domain of eRF1 with the GGQ loop close to the peptidyl tRNA (left and middle). Position and conformation of the GGQ loop are highly similar to that of bacterial RF1 (Laurberg et al., 2008).

"bolt" that transmits conformational changes within ABCE1 upon ATP hydrolysis to the ribosome and induces splitting of the subunits. More structural and biochemical data will be needed to understand how this reaction is triggered and how ordered ATP binding and ATP hydrolysis in the two NBDs of ABCE1 contribute to this process.

EXPERIMENTAL PROCEDURES

Programmed CMV-stalled RNCs were prepared from a wheat germ in-vitro-translation extract as described by Bhushan et al. (2010). Recombinant yeast eRF1, eRF3, and ABCE1 were overexpressed in *E. coli* or *S. cerevisiae* and affinity purified. For release assays, RNCs were incubated together with the ligands, and tagged nascent peptidyl tRNA or free peptide was analyzed by western blotting.

Termination complexes were formed by in vitro reconstitution with recombinant-purified factors. The complexes were vitrified, and data were collected on a Titan Krios electron microscope (FEI). Single-particle analysis followed by 3D reconstruction was performed using the SPIDER software package (Frank et al., 1996). For molecular interpretation of the *Triticum aestivum* 80S ribosome, we used an updated model (Gogala et al., 2014). Models of eRF1, eRF3, and ABCE1 were based on existing crystal structures. See Supplemental Experimental Procedures for a detailed description of the Experimental Procedures.

ACCESSION NUMBERS

Cryo-EM maps for the pretermination complex (RNC-eRF1-eRF3) and the termination/prerecycling complex (RNC-eRF1-ABCE1) have been deposited in the EMDataBank under accession codes EMD-2597 and EMD-2598. The respective coordinates for EM-based models are deposited in the Protein Data Bank under ID codes 4rcn and 4rcm.

SUPPLEMENTAL INFORMATION

Supplemental Information includes Supplemental Experimental Procedures, four figures, two tables, and one movie and can be found with this article online at http://dx.doi.org/10.1016/j.celrep.2014.04.058.

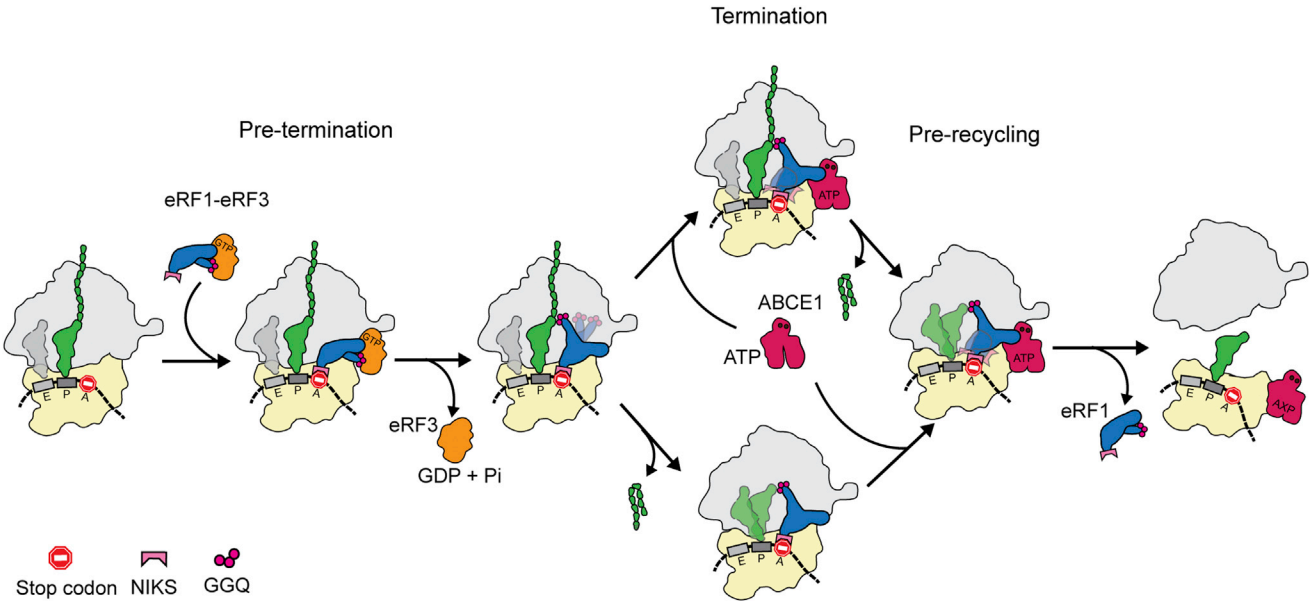

Figure 4. Scheme of Eukaryotic Translation Termination and Ribosome Recycling

For termination, the stop codon in the A site is recognized by the eRF1-eRF3-GTP ternary complex. eRF3 dissociates after GTP hydrolysis and allows the central domain of eRF1 to swing to the PTC. Proper positioning of the GGQ motif in the central domain of eRF1 may already allow peptide release, resulting in a termination complex with the deacyl-tRNA in the P state or P/E hybrid state. Alternatively, the active conformation of eRF1 in the pretermination complex is stabilized after binding of ABCE1. This stimulates peptide release while the NTD of eRF1 is delocalized, thus decoupling decoding from peptide release. Independent of the termination mechanism, ABCE1 together with eRF1 functions in concert to dissociate the ribosome into small and large subunits.

AUTHOR CONTRIBUTIONS

A.P., T.B., and R.B. designed the study. D.E.E. generated expression plasmids. A.P. carried out RNC and release factor purifications, generation of termination factor complexes, and biochemical assays. A. Heuer purified ABCE1. O.B. collected cryo-EM data. A. Hauser developed the Starfish software. A.P. and A. Heuer processed and interpreted the cryo-EM structures. T.B. built molecular models for eRF1 and eRF3. A.P. and T.B. prepared all figures. C.B.-G. built a refined model of the wheat germ ribosome. A. Heuer created Movie S1. A.P., T.B., R.B., and R.G. interpreted results and wrote the paper.

ACKNOWLEDGMENTS

We thank Charlotte Ungewickell for assistance with cryo-EM and Heidemarie Sieber for assistance with biochemical experiments. This work was supported by grants from the German Research Council (GRK 1721, FOR 1805, and SFB646 to R.B., and SFB646 to T.B). R.B. acknowledges support by the Center for Integrated Protein Science and the European Research Council (Advanced Grant CRYOTRANSLATION).

Received: January 25, 2014
Revised: March 1, 2014
Accepted: April 3, 2014
Published: July 3, 2014

REFERENCES

Alkalaeva, E.Z., Pisarev, A.V., Frolova, L.Y., Kisselev, L.L., and Pestova, T.V. (2006). In vitro reconstitution of eukaryotic translation reveals cooperativity between release factors eRF1 and eRF3. Cell *125*, 1125–1136.

Barthelme, D., Dinkelaker, S., Albers, S.V., Londei, P., Ermler, U., and Tampé, R. (2011). Ribosome recycling depends on a mechanistic link between the FeS cluster domain and a conformational switch of the twin-ATPase ABCE1. Proc. Natl. Acad. Sci. USA *108*, 3228–3233.

Becker, T., Armache, J.P., Jarasch, A., Anger, A.M., Villa, E., Sieber, H., Motaal, B.A., Mielke, T., Berninghausen, O., and Beckmann, R. (2011). Structure of the no-go mRNA decay complex Dom34-Hbs1 bound to a stalled 80S ribosome. Nat. Struct. Mol. Biol. *18*, 715–720.

Becker, T., Franckenberg, S., Wickles, S., Shoemaker, C.J., Anger, A.M., Armache, J.P., Sieber, H., Ungewickell, C., Berninghausen, O., Daberkow, I., et al. (2012). Structural basis of highly conserved ribosome recycling in eukaryotes and archaea. Nature *482*, 501–506.

Bhushan, S., Meyer, H., Starosta, A.L., Becker, T., Mielke, T., Berninghausen, O., Sattler, M., Wilson, D.N., and Beckmann, R. (2010). Structural basis for translational stalling by human cytomegalovirus and fungal arginine attenuator peptide. Mol. Cell *40*, 138–146.

Cheng, Z., Saito, K., Pisarev, A.V., Wada, M., Pisareva, V.P., Pestova, T.V., Gajda, M., Round, A., Kong, C., Lim, M., et al. (2009). Structural insights into eRF3 and stop codon recognition by eRF1. Genes Dev. *23*, 1106–1118.

des Georges, A., Hashem, Y., Unbehaun, A., Grassucci, R.A., Taylor, D., Hellen, C.U., Pestova, T.V., and Frank, J. (2014). Structure of the mammalian ribosomal pre-termination complex associated with eRF1.eRF3.GDPNP. Nucleic Acids Res. *42*, 3409–3418.

Doma, M.K., and Parker, R. (2006). Endonucleolytic cleavage of eukaryotic mRNAs with stalls in translation elongation. Nature *440*, 561–564.

Franckenberg, S., Becker, T., and Beckmann, R. (2012). Structural view on recycling of archaeal and eukaryotic ribosomes after canonical termination and ribosome rescue. Curr. Opin. Struct. Biol. *22*, 786–796.

Frank, J., Radermacher, M., Penczek, P., Zhu, J., Li, Y., Ladjadj, M., and Leith, A. (1996). SPIDER and WEB: processing and visualization of images in 3D electron microscopy and related fields. J. Struct. Biol. *116*, 190–199.

Freistroffer, D.V., Pavlov, M.Y., MacDougall, J., Buckingham, R.H., and Ehrenberg, M. (1997). Release factor RF3 in *E. coli* accelerates the dissociation of

release factors RF1 and RF2 from the ribosome in a GTP-dependent manner. EMBO J. *16*, 4126–4133.

Frolova, L., Le Goff, X., Zhouravleva, G., Davydova, E., Philippe, M., and Kisselev, L. (1996). Eukaryotic polypeptide chain release factor eRF3 is an eRF1- and ribosome-dependent guanosine triphosphatase. RNA *2*, 334–341.

Gogala, M., Becker, T., Beatrix, B., Armache, J.P., Barrio-Garcia, C., Berninghausen, O., and Beckmann, R. (2014). Structures of the Sec61 complex engaged in nascent peptide translocation or membrane insertion. Nature *506*, 107–110.

Janzen, D.M., Frolova, L., and Geballe, A.P. (2002). Inhibition of translation termination mediated by an interaction of eukaryotic release factor 1 with a nascent peptidyl-tRNA. Mol. Cell. Biol. *22*, 8562–8570.

Jenner, L., Melnikov, S., Garreau de Loubresse, N., Ben-Shem, A., Iskakova, M., Urzhumtsev, A., Meskauskas, A., Dinman, J., Yusupova, G., and Yusupov, M. (2012). Crystal structure of the 80S yeast ribosome. Curr. Opin. Struct. Biol. *22*, 759–767.

Karcher, A., Schele, A., and Hopfner, K.P. (2008). X-ray structure of the complete ABC enzyme ABCE1 from *Pyrococcus abyssi*. J. Biol. Chem. *283*, 7962–7971.

Kong, C., Ito, K., Walsh, M.A., Wada, M., Liu, Y., Kumar, S., Barford, D., Nakamura, Y., and Song, H. (2004). Crystal structure and functional analysis of the eukaryotic class II release factor eRF3 from S. pombe. Mol. Cell *14*, 233–245.

Korostelev, A., Asahara, H., Lancaster, L., Laurberg, M., Hirschi, A., Zhu, J., Trakhanov, S., Scott, W.G., and Noller, H.F. (2008). Crystal structure of a translation termination complex formed with release factor RF2. Proc. Natl. Acad. Sci. USA *105*, 19684–19689.

Kryuchkova, P., Grishin, A., Eliseev, B., Karyagina, A., Frolova, L., and Alkalaeva, E. (2013). Two-step model of stop codon recognition by eukaryotic release factor eRF1. Nucleic Acids Res. *41*, 4573–4586.

Laurberg, M., Asahara, H., Korostelev, A., Zhu, J., Trakhanov, S., and Noller, H.F. (2008). Structural basis for translation termination on the 70S ribosome. Nature *454*, 852–857.

Mantsyzov, A.B., Ivanova, E.V., Birdsall, B., Alkalaeva, E.Z., Kryuchkova, P.N., Kelly, G., Frolova, L.Y., and Polshakov, V.I. (2010). NMR solution structure and function of the C-terminal domain of eukaryotic class 1 polypeptide chain release factor. FEBS J. *277*, 2611–2627.

Pisarev, A.V., Skabkin, M.A., Pisareva, V.P., Skabkina, O.V., Rakotondrafara, A.M., Hentze, M.W., Hellen, C.U., and Pestova, T.V. (2010). The role of ABCE1 in eukaryotic posttermination ribosomal recycling. Mol. Cell *37*, 196–210.

Pisareva, V.P., Skabkin, M.A., Hellen, C.U., Pestova, T.V., and Pisarev, A.V. (2011). Dissociation by Pelota, Hbs1 and ABCE1 of mammalian vacant 80S ribosomes and stalled elongation complexes. EMBO J. *30*, 1804–1817.

Shoemaker, C.J., and Green, R. (2011). Kinetic analysis reveals the ordered coupling of translation termination and ribosome recycling in yeast. Proc. Natl. Acad. Sci. USA *108*, E1392–E1398.

Shoemaker, C.J., Eyler, D.E., and Green, R. (2010). Dom34:Hbs1 promotes subunit dissociation and peptidyl-tRNA drop-off to initiate no-go decay. Science *330*, 369–372.

Song, H., Mugnier, P., Das, A.K., Webb, H.M., Evans, D.R., Tuite, M.F., Hemmings, B.A., and Barford, D. (2000). The crystal structure of human eukaryotic release factor eRF1—mechanism of stop codon recognition and peptidyl-tRNA hydrolysis. Cell *100*, 311–321.

Taylor, D., Unbehaun, A., Li, W., Das, S., Lei, J., Liao, H.Y., Grassucci, R.A., Pestova, T.V., and Frank, J. (2012). Cryo-EM structure of the mammalian eukaryotic release factor eRF1-eRF3-associated termination complex. Proc. Natl. Acad. Sci. USA *109*, 18413–18418.

Weixlbaumer, A., Jin, H., Neubauer, C., Voorhees, R.M., Petry, S., Kelley, A.C., and Ramakrishnan, V. (2008). Insights into translational termination from the structure of RF2 bound to the ribosome. Science *322*, 953–956.

Cell Reports, Volume *8*

Supplemental Information

Cryoelectron Microscopic Structures of Eukaryotic Translation Termination Complexes Containing eRF1-eRF3 or eRF1-ABCE1

Anne Preis, Andre Heuer, Clara Barrio-Garcia, Andreas Hauser, Daniel E. Eyler, Otto Berninghausen, Rachel Green, Thomas Becker, and Roland Beckmann

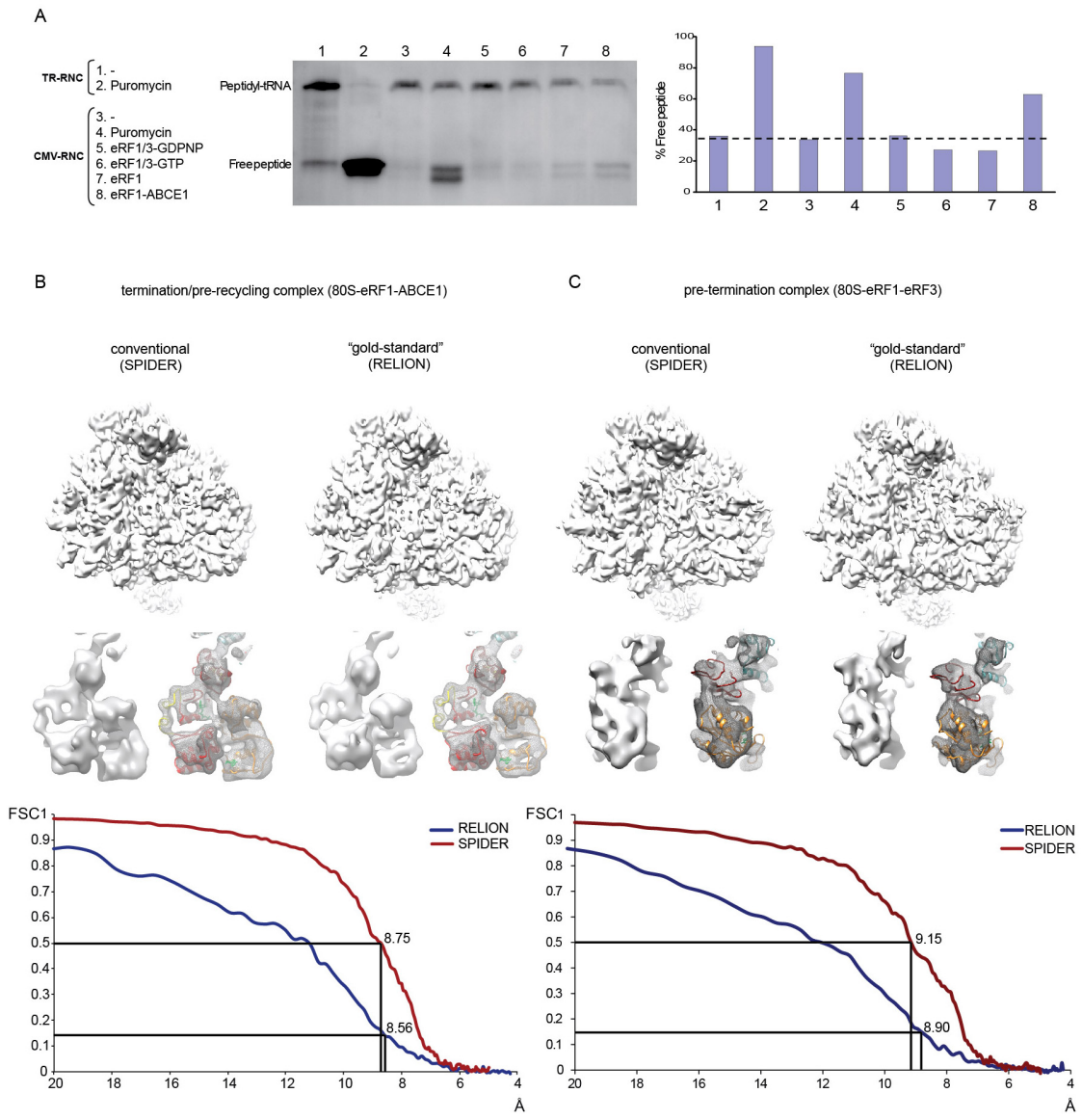

Figure S1 (related to Results and Discussion, Experimental Procedures and Figure 1) : Release Assays and Comparison between conventional refinement and "gold-standard" refinement (B,C)

"CMV-stalled" RNCs with a stop-codon in the A-site were either treated with puromycin or incubated with a 5-fold molar excess of release/recycling factor complexes and subjected to Western Blot analysis using an anti-HA antibody (**A**). Bands for peptidyl-tRNA and free peptide are indicated. As a measure for release activity the relative amount of free peptide was quantified using ImageJ. As a control, RNCs stalled by truncated mRNA (TR-RNC) were used.

Cryo-EM maps and resolution curves resulting from conventional SPIDER and "gold-standard" RELION refinement are shown for (**B**) the termination/pre-recycling dataset and (**C**) the pre-termination dataset. Snapshots were taken from the entire ribosome, the ribosomal exit site and isolated densities for the ligands (ABCE1 in (**B**), eRF3 in (**C**).

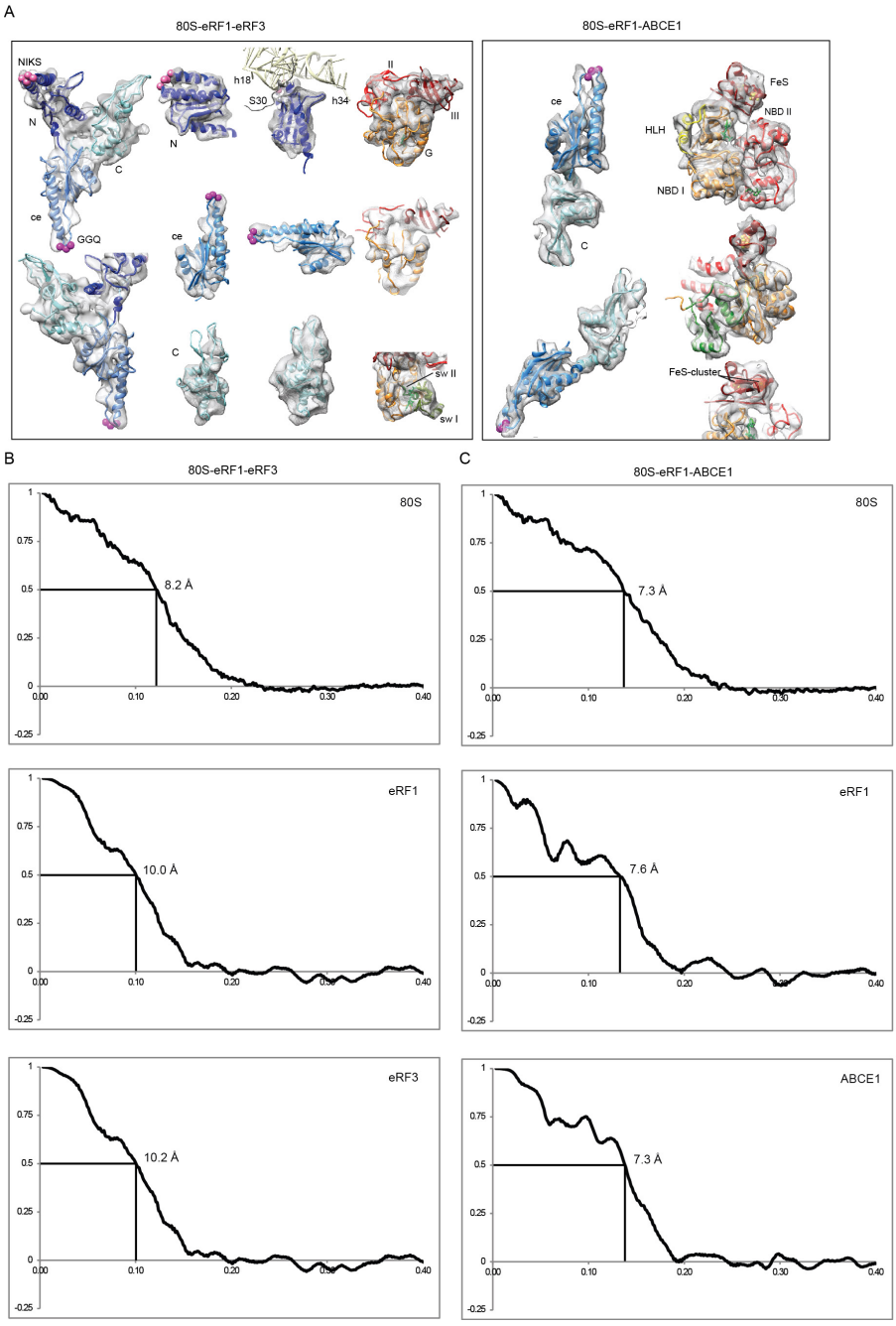

Figure S2 (related to Figures 1-3): Fitting of eRF1, eRF3 and ABCE1 and FSC curves between experimental maps and molecular models.

Isolated densities for eRF1, eRF3 and ABCE1 are shown in transperent mesh with homology models fitted based on resolved secondary structure. The color code for individual domains is as in **Figure 1B.** In addition, for the eRF1-NTD the ribosomal interaction site is shown. The mini-domain insert of the eRF1-CTD can only be seen with low contour levels. Density for the two FeS-clusters of ABCE1 is shown in red mesh. Nucleotides (GDPNP for eRF3, ATP for ABCE1) are shown in green.

FSC curves between models and maps for the 80S-eRF1-eRF3 dataset (**B**) and the 80S-eRF1-ABCE1 dataset (**C**) were calculated for the entire 80S ribosome using the model for the wheat germ ribosome (3J5Z, 3J60, 3J61 and 3J62) and for individual ligands. For ligands, respective densities were cut out using a soft mask and the resolution was read at a cutoff at a FSC 0.5.

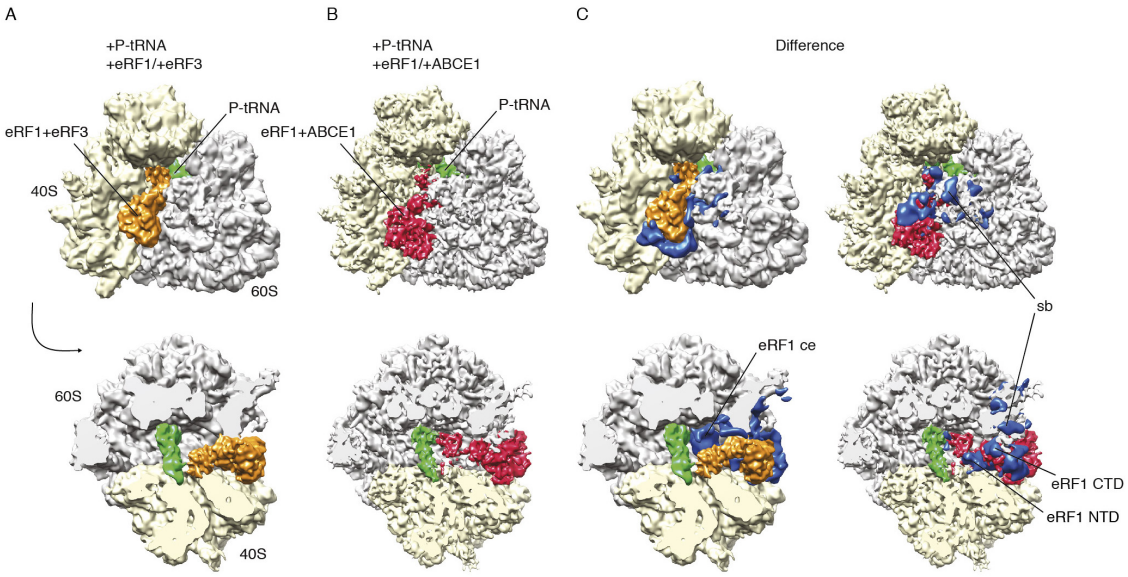

Figure S3 (related to Figure 1): Difference maps.

Front and top views of pre-termination (**A**) and termination/pre-recycling (**B**) complexes. In (**C**) the difference map of (**B**) minus (**A**) is shown in blue. Differences can be seen for the ribosomal stalk base (rRNA helices H43-H44 and r-protein L11), the eRF1 central domain and ABCE1. (**D**) represents the difference map (**A**) minus (**B**). Differences can be seen for the ribosomal stalk base (sb), eRF3 and the CTD and the NTD of eRF1.

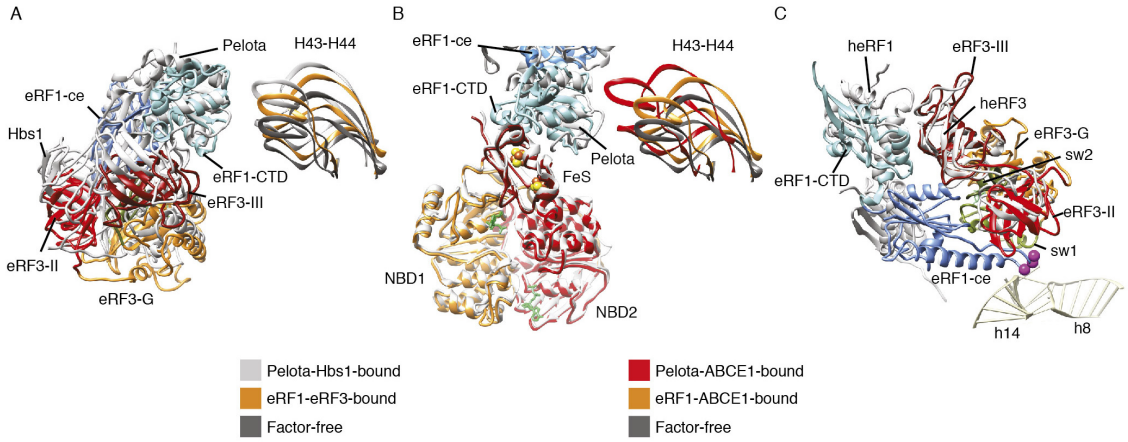

Figure S4 (related to Figures 2 and 3): Comparative analysis of ribosome-bound eRF1-eRF3 and eRF1-ABCE1 complexes.
(**A**) Overlay of the model for eRF1-eRF3 (color code as in **Figure 1B**) with Pelota-Hbs1 (PDB accession 3IZQ) (*17*) (grey). (**B**) Overlay of eRF1-ABCE1 (color code as in **Figure 1B**) with Pelota-ABCE1 (PDB accession 3J16) (*18*) (grey). The position of stalk-base helices H43-H44 in given in dark grey (factor-free), orange (bound to eRF1-eRF3), grey (bound to Pelota-Hbs1) and red (bound to eRF1-ABCE1 or Pelota-ABCE1). (**C**) Overlay of model for eRF1-eRF3 with the crystal structure of the human eRF1-eRF3 complex (PDB accession 3E1Y) (*12*) lacking the eRF3-G domain (grey).

Movie S1 (related to Figure 4): Eukaryotic translation termination.

Table S1: Contacts in the RNC-eRF1-eRF3:GDPNP pre-termination complex (related to Figure 2).

Table S2: Contacts in the RNC-eRF1-ABCE1:ADPNP termination/pre-recycling complex (related to Figure 3).

Supplemental Experimental Procedures

Purification of CMV-stalled ribosome nascent chain complexes

Wheat germ ribosomes were programmed with mRNA containing the first 98 amino acids of dipeptityl-pepdidase (DPAP-B98) carrying a type II signal anchor sequence followed by the 22-codon long human CMV *gp48* uORF stalling sequence. The template also encoded for N-terminal hexahistidine (His_6) and hemeagglutinin (HA) tags. The PCR-amplified DNA template was used for synthesis of uncapped mRNA using T7 RNA polymerase. RNCs were purified from the wheat germ cell-free translation extract as described before (Bhushan et al., 2010).

RNCs stalled by truncated mRNA coding for the first 120 amino acids of DPAP-B (DP120) were generated as described before (Becker et al., 2009).

Purification of eRF1, eRF3 and ABCE1

eRF1 and eRF3ΔN97 were cloned into pTYB2 (part of the IMPACT system by NEB) between the NdeI and SmaI sites and individually overexpressed in *E coli* BL21(DE3). Expression was carried out in Terrific Broth and induced with IPTG at 16 ºC for 15 h. Cells expressing release factors were washed with cold 1 % KCl, resuspended in lysis buffer eRF1 (20 mM HEPES pH 7.5, 500 mM NaCl, 1 mM EDTA) or lysis buffer eRF3 (20 mM HEPES pH 7.5, 500 mM NaCl, 0.1 mM GTP) and lysed using a French press.

The lysate was clarified at 20,000 g for 30 min (Beckmann Type 45 Ti) and loaded on Chitin Beads (NEB), 2 ml bed volume per 1 l of expression culture. The column was washed with 20 column volumes (CV) of corresponding lysis buffer and 20 CV of wash buffer (20 mM HEPES pH 7.5, 1 M NaCl, 1 mM EDTA). The column was flushed with 3 CV of elution buffer (20 mM HEPES pH 7.5, 500 mM KCl, 1 mM EDTA, 50 mM DTT) and incubated for 16 h at 4 ºC. The factors were eluted with 6 CV of elution buffer, concentrated and exchanged into gel filtration buffer (20mM HEPES pH 7.5, 200 mM KCl, 2 mM DTT, 1.5 mM $MgCl_2$, 10% Glycerol) in Microspin centrifugal filter units (threshold 10,000, Invitrogen) in 10-minute steps at 2500 g (5417/R, Eppendorf). Prior to gel filtration, the factors were incubated together in gel filtration buffer in the presence of 500 µM GDPNP or GTP on ice for 15 min. The complexes were purified on a Superdex 200 10/300 GL column and stored in gel filtration buffer. ABCE1 was purified from *S. cerevisiae* as described before (Shoemaker and Green, 2011).

Release assays

2 pmol RNCs were incubated with a ten-fold molar excess of eRF1-eRF3-GDPNP, eRF1 alone or eRF1 and ABCE1 in binding buffer (20 mM HEPES pH 7.5, 200 mM KCl, 1.5 $MgCl_2$, 2 mM DTT, 10 µg/ml cycloheximide, supplied with 500 µM GDPNP, GTP or ADPNP). Puromycin was added to a final concentration of 0.1 mM. The assays were incubated for 1 h at 27 ºC and analyzed by Western blot for HA-tag.

Reconstitution of RNC-eRF1-eRF3 and RNC-eRF1-ABCE1 complexes and cryo-EM sample preparation

RNCs were incubated with a ten-fold molar excess of preformed eRF1-eRF3 complex or eRF1 and ABCE1 in grid buffer (20 mM HEPES pH 7.5, 200 mM KCl, 1.5 $MgCl_2$, 2

mM DTT, 10 µg/ml cycloheximide, 0.05 % Nikkol, 0.03 % DBC, 500 µM GDPNP/ADPNP). Sec61 was added at a five-fold molar excess to saturate the hydrophobic signal-anchor sequence and avoid orientational bias on the cryo-grids.

Electron microscopy and image processing

For sample preparation, 2nm-carbon coated Quantifoil grids were used. The grids were prepared as described before (Wagenknecht et al., 1988). Both datasets were collected at 200 keV at a magnification of 147,136 × at the plane of the CCD using a TemCam-F416 CMOS camera (TVIPS GmbH, 4096 × 4096 pixel, 15.6 µm pixel, 1 s/full frame) resulting in an image pixel size of 1.06 Å (object scale). The particles were picked with starfish_boxing version 0.2.0, which is part of the new StarFish single particle analysis program suite. Starfish_boxing detects electron dense features by binarizing the raw micrographs into pixels with a value above an expected threshold and below. The binarization of the micrograph uses two arithmetic mean filtered images representing foreground and local background and are computed with either a very fast real space SSE2 implementation of with an FFT library. Only two parameters are required for a given dataset: the expected radius of the particle and a threshold for the binarization. After the binarization one usually gets many connected components ("white areas") in the shape of the densities present, e.g. particles, ice or similarly sized contamination. The connected components are then detected with a very simple algorithm. Based on the assumption that most connected components are particles a filter based on the median box size is used to filter out non-particles. The final coordinates were used for boxing out the particle images followed by import into SPIDER (Frank et al., 1996).

The RNC-eRF1-eRF3 dataset (224,689 particles) was sorted for presence of P-site tRNA first followed by sorting for the presence of factors. For the final reconstruction 39,309 particles were used. Sorting the RNC-eRF1-ABCE1 dataset (149,673 particles) was carried out analogously with 51,049 particles used for the final reconstruction.

The final datasets were also subjected to refinement using the "gold-standard" approach applied by the RELION software (Scheres, 2012). Here, the dataset is split into two data-subsets that are refined independently. The resolution was read at a FSC of 0.143 and, in good agreement with the results from conventional SPIDER processing, final resolutions after "gold-standard" processing were determined to 8.9 Å for the RNC-eRF1-eRF3 dataset and 8.6 Å for the RNC-eRF1-ABCE1 dataset.

Model building

For molecular interpretation of the *Triticum aestivum* 80S ribosome we used the updated model (pdb codes 3J5Z, 3J60, 3J61 and 3J62) (Gogala, 2014). Homology models of the central and NTD of eRF1 were built using HHPRED (Soding et al., 2005) on the basis of *Homo sapiens* and *Schizosaccaromyces pombe* crystal structures (Cheng et al., 2009; Song et al., 2000) (PDB accession 3E20 and 1DT9) The CTD (including the mini-domain insert that is not present in the crystal structures) was built on the basis of a NMR structure of the CTD of human eRF1 (PDB accession 2KTU) (Mantsyzov et al., 2010). The GGQ-loop (residues 177-183 of eRF1) was modeled based the GGQ-loop of RF2 (PDB accession 2XRT) (Jin et al., 2010) and RF1 (PDB accession 3MR8) (Korostelev et al., 2010). The eRF3 homology model was built on the basis of crystal structures of *S. pombe* Hbs1 (PDB accession 3MCA) (Chen et al., 2010) and eRF3 (PDB accession 1R5O) (Kong et al., 2004). Models for ABCE1 in the open ADP-bound, intermediate and closed ATP-bound state were described previously (Becker et al., 2012). Individual

domains of eRF1 and eRF3 were fitted as rigid bodies first and then manually adjusted using USCF Chimera (Pettersen et al., 2004) and Coot (Emsley and Cowtan, 2004). Final models were minimized in UCSF Chimera and clashes were removed using VMD (Phillips et al., 2005) and MDFF (Trabuco et al., 2008).

To validate the quality of the models the cross-resolution between the maps and the model was calculated. Using Chimera, we generated a map from the model-pdbs and calculated the resolution between these maps and our experimental maps. This was done for the entire ribosome as well as for individual factors eRF1, eRF3 and ABCE1. Isolated densities for the factors were extracted using soft masks in SPIDER.

SUPPLEMENTAL REFERENCES

Becker, T., Bhushan, S., Jarasch, A., Armache, J.P., Funes, S., Jossinet, F., Gumbart, J., Mielke, T., Berninghausen, O., Schulten, K.*, et al.* (2009). Structure of monomeric yeast and mammalian Sec61 complexes interacting with the translating ribosome. Science *326*, 1369-1373.

Chen, L., Muhlrad, D., Hauryliuk, V., Cheng, Z., Lim, M.K., Shyp, V., Parker, R., and Song, H. (2010). Structure of the Dom34-Hbs1 complex and implications for no-go decay. Nat. Struct. Mo.l Biol. *17*, 1233-1240.

Emsley, P., and Cowtan, K. (2004). Coot: model-building tools for molecular graphics. Acta. Crystallogr. D. Biol. Crystallogr. *60*, 2126-2132.

Gogala, M., Becker, T., Beatrix, B., Armache, J.-P., Barrio-Garcia, C.,Berninghausen, O. Beckmann, R. (2014). Cryo-EM structures of the Sec61-complex engaged in nascent peptide translocation or membrane insertion. Nature *506* 107-10.

Jin, H., Kelley, A.C., Loakes, D., and Ramakrishnan, V. (2010). Structure of the 70S ribosome bound to release factor 2 and a substrate analog provides insights into catalysis of peptide release. Proc. Natl. Acad. Sci. USA *107*, 8593-8598.

Korostelev, A., Zhu, J., Asahara, H., and Noller, H.F. (2010). Recognition of the amber UAG stop codon by release factor RF1. EMBO J. *29*, 2577-2585.

Pettersen, E.F., Goddard, T.D., Huang, C.C., Couch, G.S., Greenblatt, D.M., Meng, E.C., and Ferrin, T.E. (2004). UCSF Chimera--a visualization system for exploratory research and analysis. J. Comput. Chem. *25*, 1605-1612.

Phillips, J.C., Braun, R., Wang, W., Gumbart, J., Tajkhorshid, E., Villa, E., Chipot, C., Skeel, R.D., Kale, L., and Schulten, K. (2005). Scalable molecular dynamics with NAMD. J. Comput. Chem. *26*, 1781-1802.

Scheres, S.H. (2012). RELION: implementation of a Bayesian approach to cryo-EM structure determination. J. Struct. Biol. *180*, 519-530.

Trabuco, L.G., Villa, E., Mitra, K., Frank, J., and Schulten, K. (2008). Flexible fitting of atomic structures into electron microscopy maps using molecular dynamics. Structure *16*, 673-683.

Wagenknecht, T., Grassucci, R., and Frank, J. (1988). Electron microscopy and computer image averaging of ice-embedded large ribosomal subunits from Escherichia coli. J. Mol. Biol..*199*, 137-147.